PAPER

Check for updates

Bis(iminoxolene)iridium complexes over four oxidation states: from sodium–iridium bonding to ligand-centered radicals†

Kahargyan Nugraha, Thomas H. Do and Seth N. Brown [iD] *

The novel iminoquinone N-(2,6-dibromophenyl)-4,6-di-tert-butyl-2-imino-o-benzoquinone (Briq), with electron-withdrawing and only mildly bulky 2,6-dibromophenyl substituents, is metalated by the iridium(ı) complex {(coe)$_2$IrCl}$_2$ to give an inseparable mixture of (Briq)$_2$Ir, (Briq)$_2$IrCl, and (Briq)$_2$IrCl$_2$. This mixture can be funneled into a single pure compound either by exhaustive oxidation with iodobenzene dichloride to give (Briq)$_2$IrCl$_2$, or by exhaustive reduction by sodium naphthalenide to give (Briq)$_2$IrNa(THF)$_2$. The latter compound can be oxidized by one electron to give four-coordinate (Briq)$_2$Ir, or undergo two-electron oxidative addition reactions with iodine or iodomethane to yield (Briq)$_2$IrI or (Briq)$_2$IrCH$_3$. Structural data in the four different oxidation states indicate that each one-electron redox step is delocalized across the metal and iminoxolene ligand, with the redox changes becoming progressively more ligand-centered as the overall oxidation state increases. In the solid state, (Briq)$_2$IrNa(THF)$_2$ has a covalent bond between sodium and iridium (d = 2.9754(8) Å). The iridium–sodium bond partially heterolyzes in solution (ΔG° = 1.3 kcal mol^{-1} in THF-d_8), and the four-coordinate anion has been characterized in the solid as the cobaltocenium salt. The iridium–sodium bond dissociation free energy is 74.3 kcal mol^{-1}.

Introduction

Iminoxolene ligands have attracted interest as ancillary ligands because of the ready accessibility of multiple oxidation states (amidophenoxide/iminosemiquinone/iminoquinone).[1,2] The oxidation states differ in the occupancy of the molecular orbital dubbed the redox-active orbital (RAO) (Fig. 1): In the amidophenoxide, it is doubly occupied and constitutes the HOMO; in the iminosemiquinone, it is the SOMO; and in the iminoquinone, it is the LUMO. All three redox states are accessible because the RAO is moderate in energy. The RAO is thus close in energy to transition metal d orbitals, particularly those of elements in the middle of the d block. The close energy match and good spatial overlap of the RAO with d orbitals fosters highly covalent metal–ligand π bonding,[3,4] which can result in unusual patterns of reactivity.[5]

We recently reported the preparation of a number of bis (iminoxolene)iridium complexes of the sterically hindered iminoxolene ligand Diso, N-(2,6-diisopropylphenyl)-4,6-di-tert-butyl-2-imino-o-benzoquinone.[4] The complexes prepared

spanned four oxidation levels, from high-valent (Diso)$_2$IrCl$_2$ to low-valent anionic Na[(Diso)$_2$Ir].[6] We sought to assess how the steric bulk of the 2,6-diisopropylphenyl groups affected the synthesis and properties of the compounds by replacing the isopropyl substituents on the N-aryl group with smaller (and more oxidation-resistant) bromo substituents. Here we report that this novel iminoxolene ligand N-(2,6-dibromophenyl)-4,6-di-tert-butyl-2-imino-o-benzoquinone, abbreviated Briq, can support the same range of oxidation states in bis(iminoxolene) iridium compounds as its bulkier analogue Diso. The Briq ligand does significantly alter the synthetic chemistry, forming multiple products on metalation with iridium. It also fosters unusual covalent sodium–iridium bonding in the lowest-valent bis(iminoxolene)iridium complex.
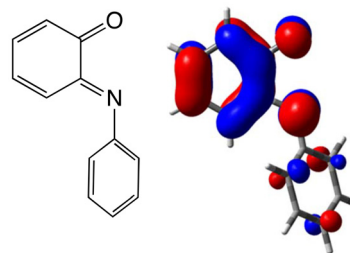
Department of Chemistry and Biochemistry, University of Notre Dame, Notre Dame, IN 46556-5670, USA. E-mail: Seth.N.Brown.114@nd.edu

Fig. 1 Redox-active orbital of N-phenyl-2-imino-o-benzoquinone (Kohn–Sham LUMO).

Experimental

General procedures

Except as noted, all procedures were carried out in a nitrogen-filled glovebox to exclude air and moisture. Deuterated solvents were obtained from Cambridge Isotope Laboratories. PhICl$_2$ was prepared as described in the literature.[7] Sodium naphthalenide was prepared as a THF solution by stirring naphthalene with 1.3 equiv. Na under N$_2$ for 3 h, then filtering through Celite. All other reagents were commercially available and used without further purification. NMR spectra were measured on a Bruker Avance DPX-400 or -500 spectrometer. Chemical shifts for ^{1}H and ^{13}C are reported in ppm downfield of TMS, with spectra referenced using the chemical shifts of the solvent residuals. Infrared spectra were recorded on a Nicolet 380 FT-IR spectrometer or a Bruker Alpha II FT-IR spectrometer. UV-visible spectra were measured in 1 cm cells on an Agilent 8453 diode array spectrophotometer. Temperatures below ambient were controlled using a Unisoku CoolSpek cryostat. Near-IR spectra were acquired on a JASCO V-770 spectrophotometer. Cyclic voltammograms were performed using an Autolab potentiostat (PGSTAT 128N), with glassy carbon working and counter electrodes and a silver/silver chloride reference electrode. The electrodes were connected to the potentiostat through electrical conduits in the drybox wall. Samples were run with 0.1 M Bu$_4$NPF$_6$ as the electrolyte. Potentials were referenced to ferrocene/ferrocenium at 0 V (ref. 8) with the reference potential established by spiking the test solution with a small amount of ferrocene or decamethylferrocene (E° = −0.565 V $vs.$ Cp$_2$Fe$^+$/Cp$_2$Fe in CH$_2$Cl$_2$ [9]). EPR spectra were measured on 1 : 1 toluene : dichloromethane glasses at 13 K using a Bruker EMX X-band spectrometer at 9.365 GHz. Elemental analyses were performed by Robertson Microlit (Ledgwood, NJ, USA) or Midwest Microlab (Indianapolis, IN, USA).

Syntheses

N-(2,6-Dibromophenyl)-4,6-di-$tert$-butyl-2-imino-o-benzoquinone (Briq). Into a screw-cap vial are weighed 0.9066 g 2,6-dibromoaniline (3.61 mmol) and 0.8731 g 3,5-di-$tert$-butyl-1,2-benzoquinone (3.96 mmol, 1.1 equiv.). After adding 4 mL glacial acetic acid, the vial is securely capped and shaken until the solids dissolve. After standing at room temperature for 6 days, the precipitated solid is suction filtered, washed with 2 × 2 mL methanol, and air-dried 30 min to afford a first crop of the iminoquinone. A second crop is obtained from the filtrate in the same manner after an additional 7 d at room temperature. After collecting the second crop, the solvent is removed from the filtrate on a rotary evaporator and the residue taken up in 4 mL CH$_3$OH. After standing for a day, the precipitated solid is isolated as described above. The total yield of the three combined crops is 0.9138 g (56%). The compound is a 53 : 47 mixture of isomers in CDCl$_3$. ^{1}H NMR (CDCl$_3$): major isomer: δ 1.12, 1.33 (s, 9H each, ^{t}Bu), 5.83, 6.98 (d, 2 Hz, 1H each, iminoquinone 3,5-H), 6.86 (t, 8 Hz, 1H, Ar 4-H), 7.55 (d, 8 Hz, 2H, Ar 3,5-H). Minor isomer: 1.18, 1.27 (s, 9H each, ^{t}Bu),

6.65, 6.96 (d, 2 Hz, 1H each, iminoquinone 3,5-H), 6.78 (t, 8 Hz, 1H, Ar 4-H), 7.51 (d, 8 Hz, 2H, Ar 3,5-H). ^{13}C{^{1}H} NMR (CDCl$_3$, both isomers): δ 28.44, 28.62, 29.42, 29.61 (C[CH_3]$_3$), 35.33, 35.57, 35.70, 35.78 (C[CH$_3$]$_3$), 110.17, 113.05, 115.13, 124.10, 124.53, 126.29, 132.13, 132.16, 133.80, 134.33, 147.43, 147.91, 149.14, 150.34, 155.45, 155.49, 158.26, 158.62, 179.41 (C=O), 183.81 (C=O). IR (ATR, cm^{-1}): 2968 (m), 1664 (s, $\nu_{C=O}$), 1626 (m), 1578 (w), 1560 (m), 1547 (w), 1479 (w), 1419 (s), 1394 (w), 1377 (m), 1284 (w), 1267 (w), 1250 (m), 1215 (m), 1196 (w), 1146 (w), 1109 (w), 1088 (w), 1072 (w), 1024 (w), 968 (w), 931 (w), 897 (s), 862 (m), 833 (w), 798 (m), 789 (w), 764 (vs), 748 (m), 739 (w), 729 (s), 669 (m). Anal. calcd for C$_{20}$H$_{23}$Br$_2$NO: C, 53.00; H, 5.12; N, 3.09. Found: C, 53.32; H, 5.31; N, 3.09.

$trans$-(Briq)$_2$IrCl$_2$. A 20 mL scintillation vial is charged with 0.6094 g {(coe)$_2$IrCl}$_2$ (0.680 mmol), 1.2832 g Briq (2.83 mmol, 4.16 equiv.) and 6 mL dry C$_6$H$_6$. The vial is securely capped, shaken vigorously to dissolve the compounds and left to stand at room temperature for 1 week. The precipitate is then collected by vacuum filtration. The solids are washed with 3 × 5 mL CH$_3$OH before drying in $vacuo$ overnight to afford 1.1405 g of a metalation mixture of (Briq)$_2$IrCl$_x$ (x = 0, 1, 2, avg. $x \approx 1.09$; 74%).

100.6 mg of this metalation mixture is treated with 13.1 mg (0.0477 mmol) of iodobenzene dichloride in 5 mL CH$_2$Cl$_2$ in a 20 mL vial. The vial is shaken until all solids are dissolved, and then removed from the drybox. After 3 h at room temperature, the vial is opened to the air and the solvent is removed on a rotary evaporator. The residue is slurried with 2 mL CH$_3$CN, and the solids are collected by vacuum filtration, washed with 2 × 5 mL CH$_3$CN, and air-dried 15 min to give 65.3 mg of (Briq)$_2$IrCl$_2$ (47% based on {(coe)$_2$IrCl}$_2$). ^{1}H NMR (CD$_2$Cl$_2$): δ 26.8 (v br), 13.49 (br, 18H, ^{t}Bu), 1.84 (br, 18H, ^{t}Bu), −4.19 (v br). IR (ATR, cm^{-1}): 3058 (w), 2959 (m), 2903 (w), 2866 (w), 2662 (w), 1590 (w), 1549 (w), 1519 (m), 1475 (m), 1427 (m), 1415 (m), 1395 (w), 1348 (s), 1283 (s), 1253 (s), 1230 (s), 1199 (s), 1181 (s), 1097 (s), 1072 (m), 1022 (s), 990 (s), 933 (m), 911 (s), 886 (s), 852 (s), 827 (w), 775 (s), 759 (m), 733 (s), 724 (s), 700 (m), 658 (m), 648 (m), 629 (w), 613 (s), 540 (s), 509 (s), 496 (s), 443 (m), 416 (s). UV-Vis-NIR (CCl$_4$): λ_{max} = 2060 nm (ε = 8700 L mol^{-1} cm^{-1}), 1693 (5250), 1406 (7300), 1155 (1670), 788 (8000), 716 (sh, 6500), 605 (13 200), 410 (8040), 318 (12 000). CV (CH$_2$Cl$_2$): 0.37, −0.38 V. Anal. calcd for C$_{40}$H$_{46}$Br$_4$Cl$_2$IrN$_2$O$_2$: C, 41.08; H, 3.96; N, 2.40. Found: C, 39.26; H, 3.71; N, 2.07.

(Briq)$_2$IrNa(THF)$_2$. The metalation mixture of (Briq)$_2$IrCl$_x$ prepared as described above (0.5158 g) is dissolved in 10 mL dry THF in a 20 mL vial. To this blue solution is added 1.7 mL of a 1.00 M solution of sodium naphthalenide in THF. The vial is capped and shaken vigorously. The reaction mixture is left to stand at room temperature for 30 min before the mixture is filtered through a plug of sand to remove NaCl. The solvent is then removed from the filtrate on the vacuum line. The solid residue is slurried in 5 mL hexanes, and the dark blue suspension filtered through a glass frit. The collected solids are washed with 2 × 5 mL hexanes before drying in $vacuo$ for 30 min to afford 0.3405 g (Briq)$_2$IrNa(THF)$_2$ as dark blue solids

(44% yield based on {(coe)$_2$IrCl}$_2$). ^{1}H NMR (CD$_3$CN): δ 8.05 (d, 8.1 Hz, 4H, NAr 3- and 5-H), 7.28 (t, 7.9 Hz, 2H, NAr 4-H), 6.67 (d, 2.2 Hz, 2H, iminoxolene 3- or 5-H), 5.47 (d, 2.2 Hz, 2H, iminoxolene 3- or 5-H), 1.86 (s, 18H, ^{t}Bu), 1.15 (s, 18H, ^{t}Bu). ^{13}C {^{1}H} NMR (CD$_3$CN): δ 170.11 (iminoxolene CO), 150.97, 140.64, 133.67, 133.65, 133.59, 131.26, 128.25, 115.85, 111.08, 66.35 (THF α-C), 36.02 (C(CH$_3$)$_3$), 34.24 (C(CH$_3$)$_3$), 32.73 (C(CH_3)$_3$), 30.79 (C(CH_3)$_3$), 26.31 (THF β-C). IR (ATR, cm^{-1}): 2950 (m), 2900 (m), 2865 (m), 1550 (m), 1457 (m), 1427 (s), 1361 (m), 1301 (s), 1256 (s), 1234 (m), 1201 (s), 1174 (s), 1110 (w), 1039 (m), 1024 (m), 996 (m), 926 (m), 903 (m), 876 (w), 856 (m), 827 (w), 766 (s), 723 (s), 673 (w), 651 (w), 632 (m), 614 (w), 546 (m), 507 (m), 460 (w), 411 (m). UV-Vis (THF, 25 °C): λ_{max} = 810 nm (ε = 4650 L mol^{-1} cm^{-1}), 664 nm (15 300 L mol^{-1} cm^{-1}). Anal. calcd for C$_{48}$H$_{62}$Br$_4$IrN$_2$NaO$_4$: C, 45.54; H, 4.94; N, 2.21. Found: C, 45.53; H, 4.59; N, 2.25.

[Cp$_2$Co][(Briq)$_2$Ir]. To a 20 mL vial, 307.7 mg of the metalation mixture of (Briq)$_2$IrCl$_x$ prepared as described above, 128.2 mg cobaltocene (0.678 mmol, 2.5 equiv. per Ir) and 10 mL benzene are added. The vial is capped and shaken vigorously, then left to stand at room temperature for 3 d. The precipitated solids are collected by suction filtration, washed with 2 × 5 mL C$_6$H$_6$ followed by 3 × 4 mL CH$_3$OH, and dried *in vacuo* overnight to afford 306.2 mg [CoCp$_2$][(Briq)$_2$Ir] as a fine turquoise powder (65% based on {(coe)$_2$IrCl}$_2$). ^{1}H NMR (CD$_3$CN): δ 8.04 (d, 8.0 Hz, 4H, NAr 3- and 5-H), 7.27 (t, 8.1 Hz, 2H, NAr 4-H), 6.67 (d, 2.2 Hz, 2H, iminoxolene 3- or 5-H), 5.66 (s, 10H, Cp$_2$Co), 5.47 (d, 2.2 Hz, 2H, iminoxolene 3- or 5-H), 1.86 (s, 18H, ^{t}Bu), 1.14 (s, 18H, ^{t}Bu). IR (ATR, cm^{-1}): 3097 (w), 2950 (m), 2902 (w), 2861 (w), 1548 (w), 1457 (w), 1422 (s), 1390 (w), 1359 (w), 1301 (s), 1277 (m), 1260 (s), 1203 (m), 1174 (w), 1141 (w), 1117 (w), 1076 (w), 1026 (m), 998 (m), 926 (m), 903 (m), 864 (m), 852 (m), 827 (w), 766 (s), 723 (s), 706 (w), 675 (w), 649 (w), 612 (w), 564 (w), 544 (m), 517 (w), 507 (w), 454 (s), 411 (w). UV-vis (THF): λ_{max} = 800 nm (ε = 8580 L mol^{-1} cm^{-1}), 680 (10 670). Anal. calcd for C$_{50}$H$_{46}$Br$_4$CoIrN$_2$O$_2$: C, 46.63; H, 4.38; N, 2.18. Found: C, 46.46; H, 4.22; N, 2.20.

(Briq)$_2$Ir. A 20 mL scintillation vial is charged with 87.2 mg (0.0689 mmol) (Briq)$_2$IrNa(THF)$_2$ and 24.1 mg (0.0938 mmol, 1.36 equiv.) silver trifluoromethanesulfonate in 6 mL benzene. The reaction mixture is then shaken vigorously and sealed before the vial is removed from the drybox and placed in a 60 °C oil bath overnight. The vial is brought back into the drybox and 5 mL CH$_2$Cl$_2$ is added. The resulting mixture is filtered through Celite and the solvent is removed from the filtrate on the vacuum line. The residue is suspended in 5 mL CH$_3$OH for 1.5 h before the mixture is filtered through a fritted glass funnel. The collected solids are washed with 2 × 5 mL CH$_3$OH before drying *in vacuo* overnight to afford 42.7 mg of (Briq)$_2$Ir (56%) as a dark blue powder. ^{1}H NMR (C$_6$D$_6$): 10.50 (br, 18H, ^{t}Bu), 0.75 (br, 2H, Ar 4-H), −1.57 (br, 4H, Ar 3,5-H), −2.40 (v br, 18H, ^{t}Bu). IR (ATR): 2954 (s), 2904 (m), 2865 (m), 1548 (m), 1519 (w), 1459 (w), 1441 (m), 1422 (s), 1383 (m), 1359 (s), 1320 (m), 1303 (m), 1258 (s), 1232 (m), 1199 (s), 1178 (m), 1160 (s), 1108 (m), 1076 (w), 1026 (m), 996 (m), 918 (m), 903 (w), 852 (m), 825 (m), 766 (s), 720 (s), 659 (w), 649

(m), 630 (m), 542 (m), 509 (m), 413 (w). UV-Vis (CH$_2$Cl$_2$): λ_{max} = 807 nm (ε = 15 400 L mol^{-1} cm^{-1}), 734 (12 100), 648 (23 300). Anal. calcd for C$_{40}$H$_{46}$Br$_4$IrN$_2$O$_2$: C, 43.73; H, 4.22; N, 2.55. Found: C, 42.10; H, 3.94; N, 2.38.

(Briq)$_2$IrI. 141.7 mg of (Briq)$_2$IrNa(THF)$_2$ (0.1119 mmol) is dissolved in 15 mL dry THF in a 100 mL round-bottom flask. A stir bar is placed in the flask and the flask is capped with a rubber septum and removed from the drybox. Into the rapidly stirring solution is injected a solution of 32.3 mg I$_2$ (0.127 mmol, 1.13 equiv.) in 10 mL dry THF. The deep purple solution is stirred for 5 min at room temperature before the flask is opened to air and the solvent removed on a rotary evaporator. The solid residue is dissolved in 15 mL CH$_2$Cl$_2$. The solution is washed with 10 mL 0.1 M aqueous thiosulfate and 10 mL water, then dried over anhydrous MgSO$_4$. After removing the dichloromethane on the rotary evaporator, the solid residue is collected to afford 102.7 mg of (Briq)$_2$IrI (75%). ^{1}H NMR (CD$_2$Cl$_2$): δ 8.00 (dd, 8.2, 1.3 Hz, 2H, Ar 3- or 5-H), 7.66 (dd, 8.1, 1.2 Hz, 2H, Ar 3- or 5-H), 7.25 (t, 8.1 Hz, 2H, Ar 4-H), 7.12 (d, 2.0 Hz, 2H, iminoxolene 3- or 5-H), 6.62 (d, 2.0 Hz, 2H, iminoxolene 3- or 5-H), 1.38 (s, 18H, ^{t}Bu), 1.27 (s, 18H, ^{t}Bu). ^{13}C{^{1}H} NMR (CD$_2$Cl$_2$): δ 180.04 (CO), 152.29, 147.46, 141.75, 138.53, 133.32, 132.77, 129.87, 124.84, 124.52, 120.79, 113.74, 35.59 (C(CH$_3$)$_3$), 35.14 (C(CH$_3$)$_3$), 30.97 (C(CH_3)$_3$), 29.84 (C(CH_3)$_3$). IR (ATR, cm^{-1}): 2956 (m), 2904 (w), 2865 (w), 1544 (m), 1457 (m), 1443 (m), 1425 (s), 1394 (m), 1383 (m), 1359 (s), 1320 (m), 1283 (m), 1250 (s), 1230 (s), 1197 (s), 1172 (s), 1108 (s), 1074 (w), 1026 (m), 1002 (m), 918 (m), 854 (m), 825 (w), 772 (s), 727 (s), 667 (s), 649 (w), 632 (w), 620 (w), 544 (m), 511 (m), 413 (m). UV-Vis (CH$_2$Cl$_2$): λ_{max} = 756 nm (ε = 24 300 L mol^{-1} cm^{-1}), 535 (12 100). Anal. calcd for the acetone solvate C$_{43}$H$_{52}$Br$_4$IIrN$_2$O$_3$: C, 40.24; H, 4.08; N, 2.18. Found: C, 40.14; H, 4.20; N, 2.00.

(Briq)$_2$IrCH$_3$. In a 20 mL scintillation vial, 97.1 mg of the metalation mixture (Briq)$_2$IrCl$_x$, 51.1 mg Cp$_2$Co (0.270 mmol, 3.2 equiv.) and 8 mL THF are combined. The vial is capped and shaken to give a dark blue solution, to which 8.5 μL (0.137 mmol, 1.60 equiv. per Ir) of CH$_3$I is added. The reaction is stirred at room temperature overnight before the vial is removed from the drybox. The reaction mixture is opened to the air and filtered through a plug of silica, eluting with THF. The dark purple eluent is collected and evaporated to dryness. The residue is slurried with 5 mL of methanol and the solids collected by suction filtration, washed with an additional 5 mL CH$_3$OH and air-dried for 30 min to yield 69.0 mg of (Briq)$_2$IrCH$_3$ as dark purple solids (72%). ^{1}H NMR (CD$_2$Cl$_2$): δ 7.91 (dd, 8.2, 1.2 Hz, 2H, NAr 3- or 5-H), 7.76 (dd, 8.1 Hz, 1.3 Hz, 2H, NAr 3- or 5-H), 7.21 (t, 8.1 Hz, 2H, NAr 4-H), 6.72 (d, 2.1 Hz, 2H, iminoxolene 3- or 5-H), 6.47 (d, 2.1 Hz, 2H, iminoxolene 3- or 5-H), 2.99 (s, 3H, IrCH_3), 1.31 (s, 18H, ^{t}Bu), 1.27 (s, 18H, ^{t}Bu). ^{13}C{^{1}H} NMR (CD$_2$Cl$_2$): δ 178.83 (iminoxolene CO), 149.76, 146.19, 140.38, 136.51, 133.06, 132.82, 129.26, 127.89, 123.27, 122.65, 112.53, 35.55 (C(CH$_3$)$_3$), 34.75 (C(CH$_3$)$_3$), 31.54 (C(CH_3)$_3$), 29.63 (C(CH_3)$_3$), −17.40 (IrCH_3). IR (ATR, cm^{-1}): 3074 (w), 2953 (m), 2903 (m), 2864 (m), 1763 (w), 1590 (w), 1544 (m), 1530 (m), 1477 (w), 1459 (m), 1441 (m), 1423 (s),

Paper

1382 (m), 1360 (m), 1308 (m), 1279 (w), 1258 (m) 1246 (m), 1226 (s), 1194 (s), 1173 (s), 1146 (m), 1108 (s), 1075 (m), 1022 (s), 1001 (m), 924 (m), 904 (m), 897 (m), 884 (m), 853 (s), 847 (m), 825 (m), 767 (s), 770 (s), 732 (m), 724 (s), 670 (m), 650 (m), 633 (m), 616 (w), 568 (w), 546 (m), 539 (m), 516 (m), 508 (m), 443 (w), 414 (m). UV-Vis (CH$_2$Cl$_2$): $\lambda_{\max}$ = 800 nm (ε = 52 200 L mol^{-1} cm^{-1}), 543 (2800), 474 (2100), 400 (1600). CV (CH$_2$Cl$_2$): 0.80, 0.21, −1.28 V. Anal. calcd for C$_{41}$H$_{49}$Br$_4$IrN$_2$O$_2$: C, 44.22; H, 4.43; N, 2.52. Found: C, 43.90; H, 4.85; N, 2.39.

Analysis of thermodynamic parameters for Ir–Na heterolysis by variable-temperature NMR spectroscopy

A solution of (Briq)$_2$IrNa(THF)$_2$ was prepared in THF-d_8 in the drybox and sealed in an NMR tube fitted with a Teflon-lined screw cap. ^{1}H NMR spectra were acquired in the range of 183–333 K. The data were fit to a model which included a linear temperature dependence of the chemical shifts of the two iminoxolene protons of the two species (eqn (1)). The actual chemical shifts were then calculated using the mole fractions of the bonded form (b) and the ion-paired form (ip) based on the equilibrium constant calculated from the modeled ΔH° and ΔS° of reaction (eqn (2)–(3)).

$$\delta_{\text{species}} = \delta_{\text{species,0C}} + \alpha_{\text{species}}(T - 273.15 \text{ K}) \quad (1)$$

$$\delta = \frac{\delta_{\text{b}}}{1 + K} + \frac{\delta_{\text{ip}}K}{1 + K} \quad (2)$$

$$K = e^{(-\Delta H^\circ + T\Delta S^\circ)/RT} \quad (3)$$

The ten parameters (δ_{0C} and α for each resonance and each species, and ΔH° and ΔS°) were optimized using unweighted least-squares fitting as implemented in the Solver routine of Microsoft Excel;[10] the spreadsheet used is included in the ESI.† Uncertainties in the fitted parameters were estimated as described in the literature.[11]

X-ray crystallography

Crystals were placed in inert oil before transferring to the N$_2$ cold stream of a Bruker Apex II CCD diffractometer. Data were reduced, correcting for absorption, using the program SADABS. Calculations used SHELXTL (Bruker AXS),[12] with scattering factors and anomalous dispersion terms taken from the literature.[13]

In (Briq)$_2$IrCH$_3$, there was a small amount of a component where the iridium was located about 0.4 Å away from the main Ir site on the vector away from the iridium–methyl bond. Only the Ir center of this component was modeled; it refined to 2.8 (2)% occupancy. The lattice methanol in (Briq)$_2$Ir·CH$_3$OH was disordered about an inversion center and was refined isotropically. All hydrogen atoms were found on difference Fourier maps and refined isotropically, with the exception of those in (Briq)$_2$IrI·C$_3$H$_6$O, the IrCH$_3$ group in (Briq)$_2$IrCH$_3$, and the methanol in (Briq)$_2$IrCl$_2$·CH$_3$OH. These hydrogens were placed in calculated positions and refined with their isotropic thermal parameters tied to the atom to which they are attached

(1.5× for CH$_3$ groups, 1.2× for all others). Further details about the structures are in Tables 1–2.

Results and discussion

Synthesis and metalation of Briq

N-Aryl-3,5-di-*tert*-butyl-2-imino-*o*-benzoquinones with 2,6-disubstituted aryl groups have typically been prepared by the carboxylic acid-catalyzed condensation of the aniline with commercially available 3,5-di-*tert*-butyl-*o*-benzoquinone.[15] This method is successful with 2,6-dibromoaniline (eqn (4)), but the reaction is quite slow, requiring weeks at room temperature in neat acetic acid. The slow rate is attributed to the electron-withdrawing character of the bromo substituents, as the sterically similar 2,6-dimethylaniline is reported to react in hours at −20 °C in methanol with traces of formic acid as catalyst.[15] Slow condensation was also observed with 2,6-bis(triisopropylsilylethynyl)aniline and was attributed to the electron-poor nature of the sp-hybridized carbon substituents.[16]

(4)
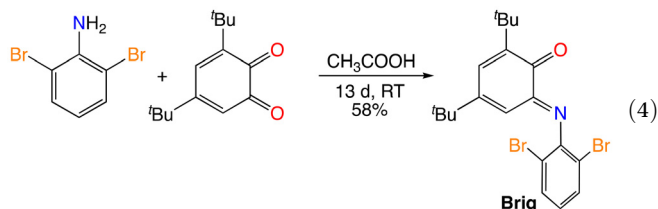
In the solid state, Briq is observed as the *E* isomer (Fig. 2), though it exists as a nearly equimolar mixture of *E* and *Z* isomers in solution. The most noteworthy feature of its structure is the appreciable twisting of the central six-membered ring out of planarity, as indicated for example by the N1–C12–C11–O1 dihedral angle of 15.7°. The other three structurally characterized *N*-aryl-*o*-benzoquinoneimines are similar, with ϕ = 10.8° for Ar = 2,6-^{i}Pr$_2$C$_6$H$_3$,[17] 15.9° for Ar = 4-CF$_3$C$_6$H$_4$,[18] and 17.2° for Ar = 2,6-(3,5-(CF$_3$)$_2$C$_6$H$_3$)$_2$C$_6$H$_3$.[19] The twisting and bond localization (Table 2) are reasonable given the formally antiaromatic 4π electron character of the central ring. The *N*-aryl substituent is significantly out of the mean plane of the iminoquinone ring, with a C12–N1–C21–C26 dihedral angle of 76.7°. This is larger than the corresponding angle for the 4-trifluoromethylphenyl group (51.1°)[18] but smaller than the value for the 2,6-diisopropylphenyl group (86.4°),[17] consistent with the steric profile of the bromo substituent being intermediate between hydrogen and isopropyl.

Treatment of benzene solutions of the iminoquinone with the iridium(I) precursor {(coe)$_2$IrCl}$_2$ (coe = η^2-cyclooctene) results in ligation of Briq to iridium and complete displacement of cyclooctene. However, in contrast to the analogous reaction of Diso, which gives diamagnetic (Diso)$_2$IrCl in high yield, the reaction of Briq gives a mixture of diamagnetic (Briq)$_2$IrCl and paramagnetic (Briq)$_2$Ir and (Briq)$_2$IrCl$_2$ (Scheme 1). A typical mixture has the three compounds in a ratio of 1.9 : 1 : 1.4 (average composition (Briq)$_2$IrCl$_{1.09}$), though this ratio varies considerably from sample to sample.

Table 1 Summary of crystal data

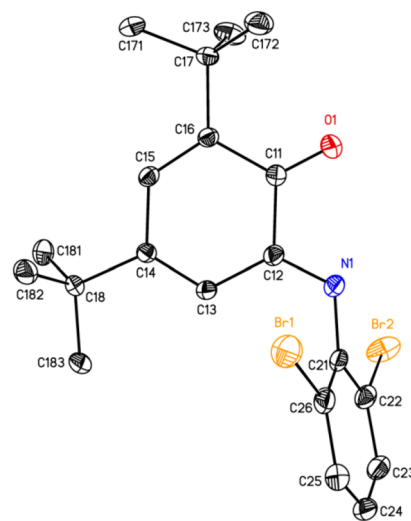|	Briq	trans-(Briq)₂IrCl₂·CH₃OH	(Briq)₂IrNa(THF)₂	[Cp₂Co][(Briq)₂Ir]·2 C₆H₆	(Briq)₂Ir·2 CHCl₃	(Briq)₂IrI·(CH₃)₂CO	(Briq)₂IrCH₃
Formula	$C_{20}H_{23}Br_2NO$	$C_{41}H_{50}Br_4Cl_2IrN_2O_3$	$C_{48}H_{62}Br_4IrN_2NaO_4$	$C_{62}H_{68}Br_4CoIrN_2O_2$	$C_{42}H_{48}Br_4Cl_6IrN_2O_2$	$C_{43}H_{52}Br_4IIrN_2O_3$	$C_{41}H_{49}Br_4IrN_2O_2$
Formula mass	453.21	1201.57	1265.82	1443.95	1337.36	1283.60	1113.66
T/K	120(2)	120(2)	120(2)	120(2)	120(2)	120(2)	120(2)
Crystal system	Monoclinic	Triclinic	Monoclinic	Monoclinic	Monoclinic	Orthorhombic	Monoclinic
Space group	$P2_1/c$	$P\bar{1}$	$C2/c$	$P2_1/c$	$P2_1/c$	$P2_12_12_1$	$P2_1/c$
λ/Å	0.71073 (Mo Kα)	0.71073 (Mo Kα)	1.54178 (Cu Kα)	0.71073 (Mo Kα)	0.71073 (Mo Kα)	0.71073 (Mo Kα)	0.71073 (Mo Kα)
Total data collected	36 428	21 734	119 244	205 171	32 230	113 473	107 470
No. of indep reflns.	4811	5631	9632	14 275	5950	12 542	12 812
R_{int}	0.0211	0.0148	0.0427	0.0847	0.0308	0.0666	0.0476
Obsd refls [$I > 2\sigma(I)$]	4350	5410	9432	11 355	5245	11 573	10 938
a/Å	12.1021(17)	10.2904(14)	29.8280(13)	13.7924(5)	15.6386(4)	10.202(2)	14.4389(12)
b/Å	11.6583(16)	11.1541(15)	18.3608(13)	19.3444(6)	10.6069(3)	15.082(3)	10.0550(8)
c/Å	13.935(2)	11.6974(16)	19.4665(10)	22.2366(8)	14.7633(4)	29.489(6)	29.257(2)
α/°	90	65.495(2)	90	90	90	90	90
β/°	99.375(2)	67.090(2)	114.354(2)	104.2700(10)	101.7892(9)	90	101.060(2)
γ/°	90	80.666(2)	90	90	90	90	90
V/Å³	1939.8(5)	1125.3(3)	9712.5(10)	5749.8(3)	2397.24(11)	4537.4(16)	4168.8(6)
Z	4	1	8	4	2	4	4
μ mm⁻¹	4.185	6.673	9.609	5.424	6.490	7.184	7.072
Crystal size/mm	0.22 × 0.32 × 0.41	0.11 × 0.28 × 0.29	0.05 × 0.11 × 0.12	0.08 × 0.11 × 0.22	0.13 × 0.14 × 0.18	0.12 × 0.14 × 0.20	0.08 × 0.16 × 0.23
No. refined params	309	334	789	873	355	487	640
R1, wR2 [$I > 2\sigma(I)$]	0.0210, 0.0524	0.0167, 0.0407	0.0169, 0.0422	0.0317, 0.0575	0.0214, 0.0439	0.0375, 0.0971	0.0288, 0.0587
R1, wR2 [all data]	0.0251, 0.0542	0.0180, 0.0414	0.0176, 0.0424	0.0501, 0.0631	0.0279, 0.0459	0.0423, 0.0991	0.0398, 0.0617
Goodness of fit	1.041	1.037	1.119	1.013	1.054	1.058	1.095

Fig. 2 Thermal ellipsoid plot of Briq (50% ellipsoids), with hydrogen atoms omitted for clarity.

The distribution of compounds appears to be kinetically controlled, as it is unchanged on heating the isolated metalation mixture.

We have not been able to separate the components of this mixture. To obtain pure compounds, we adopted a strategy of normalizing the oxidation states by exhaustive oxidation. Thus, trans-(Briq)₂IrCl₂ is isolated in 47% yield based on {(coe)₂IrCl}₂ by treatment of the metalation mixture with excess PhICl₂ (Scheme 1). The broadness and paucity of peaks in the ¹H NMR spectrum of this paramagnetic substance makes it useless for determining stereochemistry, but the similarity of the compound's UV-Vis-NIR spectrum (Fig. S20†) to that of trans-(Diso)₂IrCl₂ and its solid-state structure (Fig. 3) confirm the trans geometry.

Because the electron density on the iminoxolene ligand in the redox-active orbital affects the intraligand bond lengths, analysis of these bond lengths can be used to determine an apparent or metrical oxidation state (MOS) of the iminoxolene.[14] Such an analysis on (Briq)₂IrCl₂ gives a MOS of −0.83 (4) for each iminoxolene group, corresponding to a nominal oxidation state of iridium of close to +4. Nevertheless, the unpaired electron appears to be in a ligand-centered orbital, judging from the EPR spectrum (Fig. 4a), which shows a rhombic signal with little anisotropy (g = 2.0533, 1.9963, 1.9672; g_{iso} = 2.0059) and no resolvable hyperfine coupling. This is consistent with the SOMO being the A_u-symmetry combination of ligand RAOs, which corresponds to the HOMO of octahedral compounds such as trans-(Diso)₂IrCl(py).[20]

Preparation of (Briq)₂IrNa(THF)₂ and the nature of the sodium–iridium bonding

The oxidation states of the metalation mixture can also be normalized by exhaustive reduction. Thus, treatment of the metalation mixture with excess sodium naphthalenide results in formation of (Briq)₂IrNa(THF)₂ (Scheme 1).

Table 2 Selected distances, angles, and metrical oxidation states of iminoxolene ligands of Briq, $(Briq)_2IrNa(THF)_2$, $[Cp_2Co][(Briq)_2Ir]$, $(Briq)_2Ir$, $(Briq)_2IrCH_3$, $(Briq)_2IrI$, and $trans$-$(Briq)_2IrCl_2$. Values given are the average of chemically equivalent measurements, with esd's reflecting both the variance in the measured values and the statistical uncertainty of the crystallographic model

	Briq	$(Briq)_2IrNa(THF)_2$	$[Cp_2Co][(Briq)_2Ir]$	$(Briq)_2Ir$	$(Briq)_2IrCH_3$	$(Briq)_2IrI$	$trans$-$(Briq)_2IrCl_2$
Distances/Å							
Ir–O1		1.993(2)	2.001(13)	1.9548(16)	1.992(3)	1.997(10)	2.0022(14)
Ir–N1		1.933(3)	1.935(6)	1.936(2)	1.954(3)	1.952(10)	2.0090(15)
Ir–X		2.9754(8)			2.105(4)	2.6322(9)	2.3371(5)
O1–C11	1.2134(18)	1.330(6)	1.330(4)	1.343(3)	1.320(4)	1.312(12)	1.297(2)
N1–C12	1.2863(18)	1.391(6)	1.389(4)	1.386(3)	1.375(7)	1.358(10)	1.338(2)
C11–C12	1.531(2)	1.418(4)	1.417(7)	1.416(3)	1.418(4)	1.417(13)	1.450(3)
C12–C13	1.4469(19)	1.401(3)	1.393(4)	1.396(3)	1.405(4)	1.416(19)	1.419(3)
C13–C14	1.3456(19)	1.390(4)	1.389(6)	1.391(3)	1.375(4)	1.377(16)	1.364(3)
C14–C15	1.4686(19)	1.418(3)	1.417(5)	1.405(4)	1.420(4)	1.422(12)	1.441(3)
C15–C16	1.3474(19)	1.388(3)	1.389(5)	1.395(4)	1.383(5)	1.380(13)	1.374(3)
C11–C16	1.4824(19)	1.414(4)	1.414(4)	1.406(3)	1.421(5)	1.423(12)	1.427(3)
Angles/°							
O1–Ir–N1		79.96(14)	80.08(16)	81.19(8)	80.11(9)	79.5(6)	79.08(6)
O1–Ir–O2		179.23(5)	178.92(9)	180	178.85(10)	174.5(3)	180
N1–Ir–N2		175.77(6)	178.04(10)	180	168.21(11)	157.9(3)	180
Metrical oxidation state (MOS)[14]	+0.28(7)	−1.52(8)	−1.54(7)	−1.67(2)	−1.33(6)	−1.21(7)	−0.83(4)
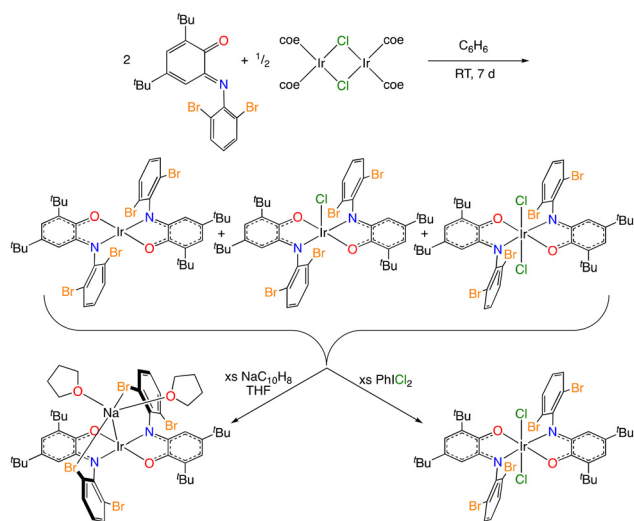
Scheme 1 Metalation of Briq and subsequent normalization of oxidation states of the metalation mixture.

Fig. 4 X-band EPR spectrum of (a) $(Briq)_2IrCl_2$ and (b) $(Briq)_2Ir$ (13 K, CH_2Cl_2/toluene glass).

Fig. 3 Thermal ellipsoid plot (50% ellipsoids) of *trans*-$(Briq)_2IrCl_2$·CH_3OH, with lattice solvent and hydrogen atoms omitted for clarity.
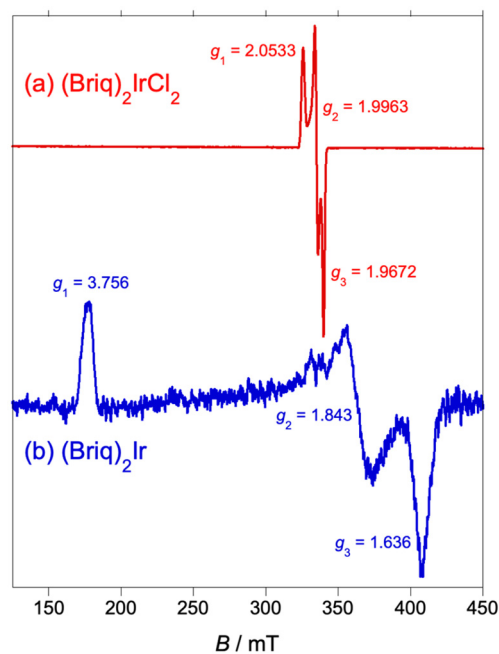
Remarkably, the complex in the solid state (Fig. 5) features a direct sodium–iridium bond (d = 2.9754(8) Å, Table 2). Alkali metal–iridium bonds are very rare. This appears to be the first example of a structurally characterized sodium–iridium bond, and the only alkali metal–iridium bond previously observed in the solid state is the potassium–iridium bond of 3.299(3) Å in K[(bpa−2H)Ir(cod)].[21] The potassium compound is a coordination polymer, with the potassium bonded in an η^5 fashion to the IrN_2C_2 rings of two doubly deprotonated dipicolylamine ligands; the K–N and K–C distances are all shorter than the K–Ir distance. In contrast, in $(Briq)_2IrNa(THF)_2$, the Na atom is
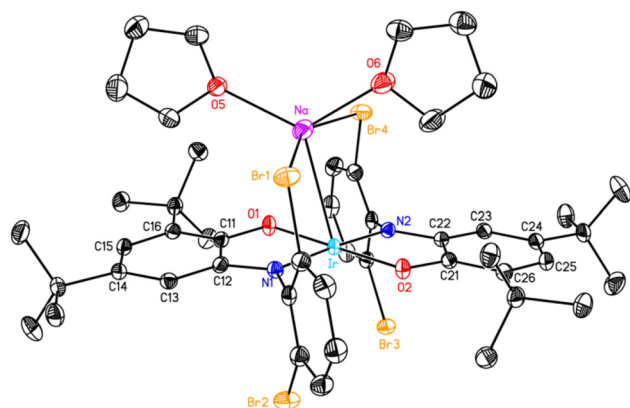
Fig. 5 Thermal ellipsoid plot (50% ellipsoids) of (Briq)$_2$IrNa(THF)$_2$, with hydrogen atoms omitted for clarity.

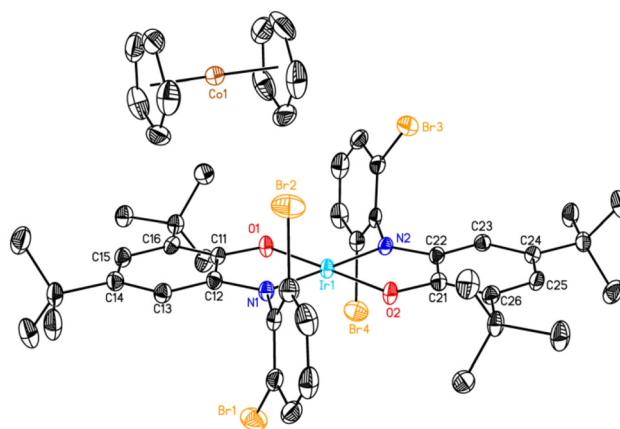**Fig. 6** Thermal ellipsoid plot (50% ellipsoids) of [Cp$_2$Co][(Briq)$_2$Ir]·2 C$_6$H$_6$, with lattice solvents and hydrogen atoms omitted for clarity.

canted toward one of the iminoxolene oxygens (O1), but the distance is very long (2.9842(16) Å), and the distances to the other atoms in the iminoxolene are all greater than 3.4 Å. Thus, the sodium is best considered bonded only to the iridium and not to the iminoxolenes. The coordination sphere of the sodium is completed by two bound THF molecules and two dative bonds from the *o*-Br substituents of the Briq ligand. The average Na–Br distance is similar to those observed in other species with sodium–bromoarene interactions (Table 3).[22]

Based on structural data, the sodium–iridium bond appears to have substantial covalency. The average unsupported metal–metal bond between neutral iridium(II) centers has a distance of 2.74(6) Å (9 examples).[23] Combined with the Na–Na distance in gas-phase Na$_2$ (3.0789 Å),[24] this would predict an Ir–Na covalent bond distance of 2.91(3) Å, within three standard deviations of the observed value. In contrast, the Na–Br distances in (Briq)$_2$IrNa(THF)$_2$ (3.09 Å avg) are much longer than the average between the homodiatomic molecules (2.68 Å), as expected for a dative bond.

If (Briq)$_2$IrCl$_x$ is reduced in the absence of an alkali metal, for example by cobaltocene, then the ionic compound [Cp$_2$Co][(Briq)$_2$Ir], containing a square planar anion, is produced (Fig. 6). This compound is structurally analogous to that

observed with the 2,6-diisopropylphenyl-substituted iminoxolene Diso, [Na(acetone)$_6$][(Diso)$_2$Ir].[6] Presumably the greater bulk of the isopropyl group and the lack of a Lewis basic site near the iridium precludes the possibility of sodium–iridium bonding in the latter compound. The geometric parameters of the four-coordinate iridium center in [Cp$_2$Co][(Briq)$_2$Ir] are remarkably similar to those in (Briq)$_2$IrNa(THF)$_2$ (Table 2). In particular, the MOS of the Briq ligand in [Cp$_2$Co][(Briq)$_2$Ir], −1.54(7), is identical within experimental error to that in (Briq)$_2$IrNa(THF)$_2$.

Consistent with the ease of formation of a four-coordinate anion, the sodium–iridium bond in (Briq)$_2$IrNa(THF)$_2$ appears to be susceptible to heterolysis in solution. In the nonpolar solvent toluene-d_8, ^{1}H NMR spectra of (Briq)$_2$IrNa(THF)$_2$ display C_2 symmetry up to 110 °C (Fig. S28†), consistent with retention of the Ir–Na bond in solution. In contrast, NMR spectra in THF-d_8 or CD$_3$CN show C_{2h} symmetry (Fig. S4†), consistent with either rapid Na$^+$ exchange between faces of a bonded complex or net formation of a solvent-separated ion pair in solution. Variable-temperature UV-vis spectroscopy in THF (Fig. 7) indicates that there is a temperature-dependent equilibrium between the bonded and the ion-pair form (eqn (5)). The former is favored at higher temperatures and the latter at low temperatures, as judged by the similarity of the low-temperature spectra to Cp$_2$Co[(Briq)$_2$Ir] (Fig. S21†). ^{1}H NMR spectroscopy shows analogous behavior, with sigmoidal dependence of chemical shifts with temperature (Fig. 8), consistent with a temperature-dependent equilibrium. Quantitative analysis of the chemical shifts gives thermodynamic parameters for eqn (5) as ΔH° = −7.3(6) kcal mol^{-1} and ΔS° = −29(2) cal mol^{-1} K^{-1}. The decrease in entropy on ionization is expected, as the combined effect of creating ions (which orders the surrounding solvent more than that surrounding neutral solutes) and coordinating additional THF to the sodium ion (there are 5–6 molecules of THF in the first coordination sphere of sodium ion[25]) outweighs the dissociation of the sodium from the iridium complex.

Table 3 Structural data regarding the sodium coordination in (Briq)$_2$IrNa(THF)$_2$

	Distance/Å		Angle/°
		Ir–Na–Br1	82.07(2)
		Ir–Na–Br4	83.11(2)
Na–Ir	2.9754(8)	Ir–Na–O5	131.21(5)
Na–Br1	3.1477(9)	Ir–Na–O6	107.84(5)
Na–Br4	3.0299(9)	Br1–Na–Br4	155.32(3)
Na–O5	2.2930(16)	Br1–Na–O5	90.95(4)
Na–O6	2.3149(19)	Br1–Na–O6	85.59(5)
		Br4–Na–O5	113.62(5)
		Br4–Na–O6	80.32(5)
		O5–Na–O6	119.73(6)
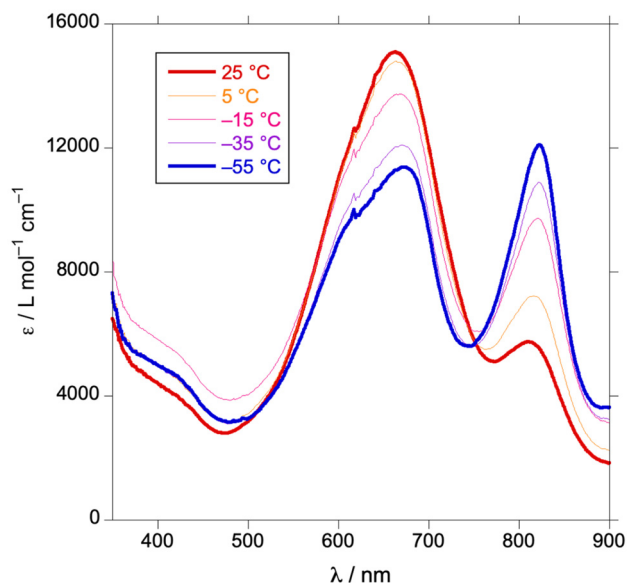
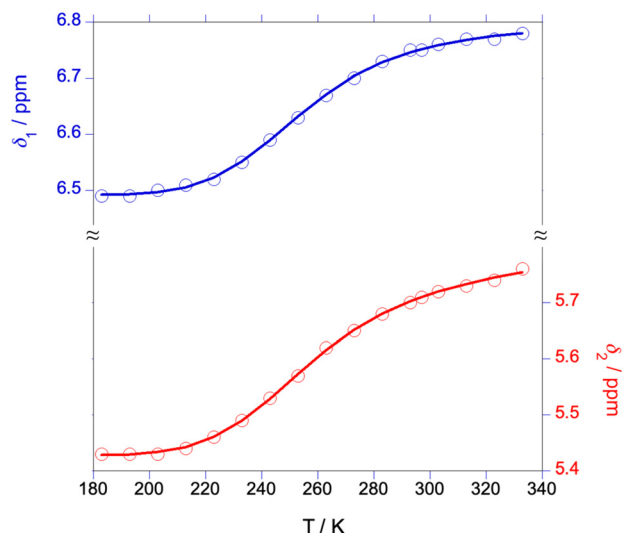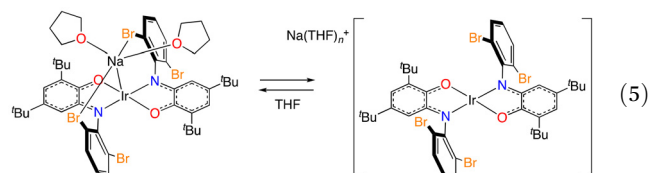**Fig. 7** Variable-temperature optical spectra of (Briq)$_2$IrNa(THF)$_2$ in THF.

Fig. 8 Chemical shifts of the iminoxolene ring protons of (Briq)$_2$IrNa (THF)$_2$ in THF-d_8. Solid lines are the best fit to eqn (1)–(3).


By combining the thermodynamics of heterolysis, the reduction potentials of (Briq)$_2$Ir and of Na$^+$, and the energies of vaporization and solvation of Na, one can calculate the thermodynamic parameters for the homolysis of the Na–Ir bond in (Briq)$_2$IrNa(THF)$_2$ in THF solution (eqn (6); see ESI† for details). The free energy change of this reaction is the Na–Ir bond dissociation free energy (BDFE) in THF solution. The

BDFE of 74.3 kcal mol^{-1} is much larger than the free energy of heterolysis (1.3 kcal mol^{-1}), as expected given the difficulty of reducing Na$^+$ to Na atoms.
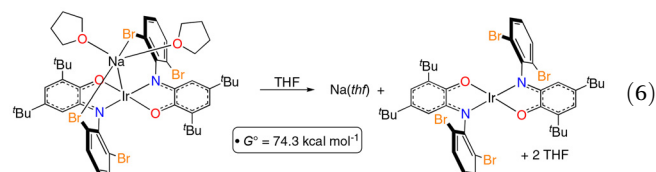
Oxidations of (Briq)$_2$IrNa(THF)$_2$

Oxidation of the low-valent complex (Briq)$_2$IrNa(THF)$_2$ is a convenient way to make other bis(iminoxolene)iridium compounds in pure form. For example, treatment of (Briq)$_2$IrNa (THF)$_2$ with ferrocenium hexafluorophosphate or with silver trifluoromethanesulfonate affords the one-electron oxidation product, neutral (Briq)$_2$Ir (eqn (7)). In the reaction with silver(I) salts, a diamagnetic C_2-symmetric intermediate, tentatively assigned as (Briq)$_2$IrAg, can be observed by NMR at short reaction times at room temperature. Silver salts of weakly coordinating anions are known to form Ag–Ir bonds with Vaska's complex, where the square planar geometry of (Ph$_3$P)$_2$Ir(CO)Cl is only minimally perturbed by the binding of the Ir d_{z^2} orbital to Ag.[26] A tris(isonitrile)iridium(−1) anion forms an unsupported Ir–Tl bond, whereas the potassium salt does not show metal–metal bonding.[27]
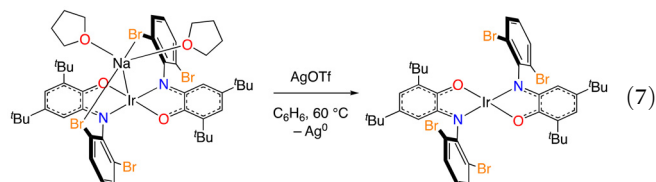
Neutral (Briq)$_2$Ir is a four-coordinate, square planar monomer (Fig. 9). The metrical oxidation state of its iminoxolene ligands is similar to those in the sodium compound, or if
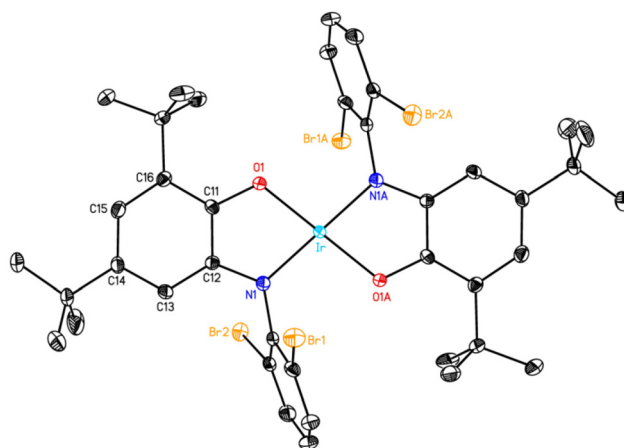

Fig. 9 Thermal ellipsoid plot of (Briq)$_2$Ir·2 CHCl$_3$ (50% ellipsoids), with solvent molecules and hydrogen atoms omitted for clarity.

anything slightly more reduced in the neutral compound ($-1.67(2)$ *vs.* $-1.52(8)$ in $(Briq)_2IrNa(THF)_2$). This suggests that oxidation takes place essentially only on the metal, consistent with an EPR spectrum that is consistent with a metal-centered radical ($g = 3.756, 1.843, 1.636$; Fig. 4b). These features, as well as its optical spectrum and paramagnetic NMR spectrum, are all similar to $(Diso)_2Ir$, which has been previously characterized as having its unpaired electron in a metal $d\pi$ orbital.[4]

The sodium–iridium complex $(Briq)_2IrNa(THF)_2$ also undergoes net two-electron oxidative addition reactions. For example, it reacts with iodine to give square pyramidal $(Briq)_2IrI$ (eqn (8)). This reaction likely proceeds *via* two one-electron steps, as neutral $(Briq)_2Ir$ reacts with I_2 to give the five-coordinate iodide complex. The iridium-sodium complex, or more conveniently the cobaltocenium salt $[Cp_2Co][(Briq)_2Ir]$, reacts with methyl iodide to afford the iridium methyl complex $(Briq)_2IrCH_3$ (eqn (9)). This likely occurs by a two-electron S_N2 pathway, as has been demonstrated for the analogous $[(Diso)_2Ir]^-$.[6]

$$(8)$$

$$(9)$$
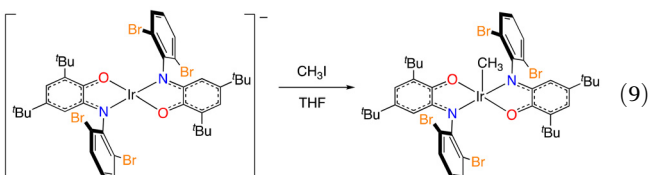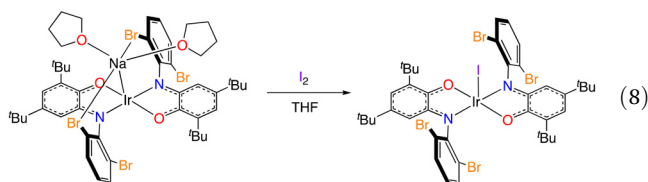
Structurally, both $(Briq)_2IrI$ (Fig. 10) and $(Briq)_2IrCH_3$ (Fig. 11) are square pyramidal (Reedijk τ_5 values[28] of 0.28 and 0.18, respectively). The metrical oxidation states of the iminoxolene ligands ($-1.21(7)$ and $-1.33(6)$, respectively) are slightly different, suggestive of a more electron-rich iminoxolene in the alkyl complex. This pattern has previously been noted between bis(iminoxolene)iridium and -cobalt halide and alkyl complexes.[6] The difference may be due to enhanced π
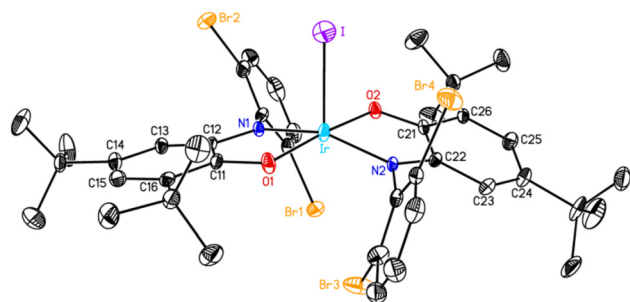

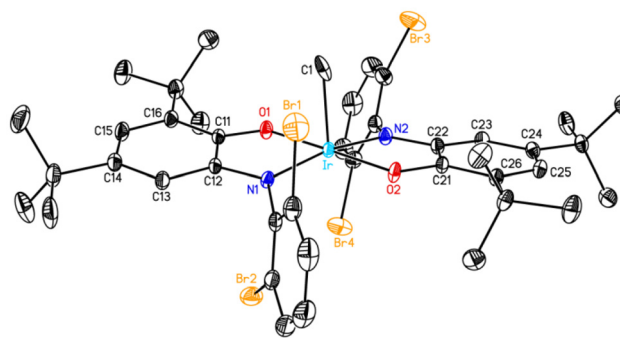**Fig. 11** Thermal ellipsoid plot of $(Briq)_2IrCH_3$ (50% ellipsoids), with hydrogen atoms omitted for clarity.

donation from the iminoxolene orbitals to the Ir–X σ^* orbital in the halides compared to the alkyls.

Overall, the iminoxolene ligands in the two $(Briq)_2IrX$ compounds (average MOS = -1.27) are significantly oxidized compared to those in $(Briq)_2Ir^-$ and $(Briq)_2Ir$ (average MOS = -1.58). This is part of a consistent trend that as the overall oxidation state of the complex becomes more positive, the oxidations become increasingly ligand-centered. Thus, the one-electron oxidation from $(Briq)_2Ir^-$ to $(Briq)_2Ir$ is essentially localized on the metal; from $(Briq)_2Ir$ to $(Briq)_2IrX$ is about 60% ligand-centered; and from $(Briq)_2IrX$ to $(Briq)_2IrCl_2$ is about 90% ligand-centered.

Conclusions

The 2,6-dibromophenyl-substituted iminoquinone Briq is metalated with an iridium(I) chloride precursor to give an inseparable mixture of $(Briq)_2Ir$, $(Briq)_2IrCl$, and $(Briq)_2IrCl_2$. This mixture can be transformed into a single oxidation state either by exhaustive oxidation (to give pure $(Briq)_2IrCl_2$) or exhaustive reduction (to give pure $[(Briq)_2Ir]^-$). Compounds with intermediate oxidation states can be prepared from the anion by one-electron (to give $(Briq)_2Ir$) or two-electron (to give $(Briq)_2IrI$ or $(Briq)_2IrCH_3$) redox reactions. In this way a suite of $(Briq)_2Ir$ complexes in four oxidation states can be accessed. Structural data indicate that each successive oxidation becomes increasingly localized at the ligands, with the $(Briq)_2Ir^-/(Briq)_2Ir$ oxidation being essentially localized at the metal, while the $(Briq)_2IrX/(Briq)_2IrCl_2$ oxidation is about 90% ligand-centered. If exhaustive reduction is carried out using sodium naphthalenide, a compound containing a covalent sodium–iridium bond, $(Briq)_2IrNa(THF)_2$, is formed. The Na–Ir bond is retained in nonpolar organic solvents but dissociates readily in more polar solvents. A bond dissociation free energy of 74.3 kcal mol^{-1} can be calculated for the sodium–iridium bond in THF solution.

Fig. 10 Thermal ellipsoid plot of $(Briq)_2IrI\cdot(CH_3)_2CO$ (50% ellipsoids), with lattice solvent and hydrogen atoms omitted for clarity.

Data availability

Crystallographic data have been deposited with the CCDC for Briq (accession number 2417993), $(Briq)_2Ir\cdot2CHCl_3$ (2417994),

(Briq)$_2$IrI·(CH$_3$)$_2$CO (2417995), (Briq)$_2$IrCH$_3$ (2417996), (Briq)$_2$IrNa(THF)$_2$ (2417997), *trans*-(Briq)$_2$IrCl$_2$·CH$_3$OH (2417998) and [Cp$_2$Co][(Briq)$_2$Ir]·2C$_6$H$_6$ (2417999).† Other data supporting this article are included as part of the ESI.†

Conflicts of interest

There are no conflicts to declare.

Acknowledgements

References

1 D. L. J. Broere, R. Plessius and J. I. van der Vlugt, *Chem. Soc. Rev.*, 2015, **44**, 6886–6915.

2 R. F. Munhá, R. A. Zarkesh and A. F. Heyduk, *Dalton Trans.*, 2013, **42**, 3751–3766.

3 J. Gianino and S. N. Brown, *Dalton Trans.*, 2020, **49**, 7015–7027.

4 T. H. Do and S. N. Brown, *Inorg. Chem.*, 2022, **61**, 5547–5562.

5 A. N. Erickson, J. Gianino, S. J. Markovitz and S. N. Brown, *Inorg. Chem.*, 2021, **60**, 4004–4014.

6 M. Meißner, K. Nugraha, K. D. Grandstaff, T. H. Do, C. A. Jiménez, W. Y. Chin, L. E. Farrell, P. D. Nguyen and S. N. Brown, *Organometallics*, 2025, **44**, DOI: **10.1021/acs.organomet.4c00514**.

7 J. Tao, R. Tran and G. K. Murphy, *J. Am. Chem. Soc.*, 2013, **135**, 16312–16315.

8 N. G. Connelly and W. E. Geiger, *Chem. Rev.*, 1996, **96**, 877–910.

9 D. Lionetti, A. J. Medvecz, V. Ugrinova, M. Quiroz-Guzman, B. C. Noll and S. N. Brown, *Inorg. Chem.*, 2010, **49**, 4687–4697.

10 D. C. Harris, *J. Chem. Educ.*, 1998, **75**, 119–121.

11 R. de Levie, *J. Chem. Educ.*, 1999, **76**, 1594–1598.

12 G. M. Sheldrick, *Acta Crystallogr., Sect. A: Found. Crystallogr.*, 2008, **A64**, 112–122.

13 *International Tables for Crystallography*, ed. A. J. C. Wilson, Kluwer Academic Publishers, Dordrecht, The Netherlands, 1992, vol. C.

14 S. N. Brown, *Inorg. Chem.*, 2012, **51**, 1251–1260.

15 G. A. Abakumov, N. O. Druzhkov, Y. A. Kurskii and A. S. Shavyrin, *Russ. Chem. Bull.*, 2003, **52**, 712–717.

16 D. A. Haungs and S. N. Brown, *Organometallics*, 2022, **41**, 3612–3626.

17 G. A. Abakumov, V. K. Cherkasov, A. V. Piskunov, I. N. Meshcheryakova, A. V. Maleeva, A. I. Poddel'skii and G. K. Fukin, *Dokl. Chem.*, 2009, **427**, 168–171.

18 A. N. Erickson and S. N. Brown, *Dalton Trans.*, 2018, **47**, 15583–15595.

19 P. R. H. Ayson and S. N. Brown, *Chem. Commun.*, 2023, **59**, 9618–9621.

20 T. H. Do, D. A. Haungs, W. Y. Chin, J. T. Jerit, A. VanderZwaag and S. N. Brown, *Inorg. Chem.*, 2023, **62**, 11718–11730.

21 C. Tejel, M. A. Ciriano, M. P. del Río, D. G. H. Hetterscheid, N. Tsichlis i Spithas, J. M. M. Smits and B. de Bruin, *Chem. – Eur. J.*, 2008, **14**, 10932–10936.

22 (*a*) K. Molčanov, B. Kojić-Prodić, D. Babić, D. Žilić and B. Rakvin, *CrystEngComm*, 2011, **13**, 5170–5178; (*b*) L. Chen, W.-K. Dong, H. Zhang, Y. Zhang and Y.-X. Sun, *Cryst. Growth Des.*, 2017, **17**, 3636–3648; (*c*) W. Cañon-Mancisidor, S. G. Miralles, J. J. Baldovi, G. M. Espallargas, A. Gaita-Ariño and E. Coronado, *Inorg. Chem.*, 2018, **57**, 14170–14177.

23 (*a*) P. G. Rasmussen, J. E. Anderson, O. H. Bailey, M. Tamres and J. C. Bayón, *J. Am. Chem. Soc.*, 1985, **107**, 279–281; (*b*) D. M. Heinekey, D. A. Fine, T. G. P. Harper and S. T. Michel, *Can. J. Chem.*, 1995, **73**, 1116–1125; (*c*) H. Hückstädt and H. Homborg, *Z. Anorg. Allg. Chem.*, 1997, **623**, 369–378; (*d*) D. M. Heinekey, D. A. Fine and D. Barnhart, *Organometallics*, 1997, **16**, 2530–2538; (*e*) S. K. Patra, S. M. W. Rahaman, M. Majumdar, A. Sinha and J. K. Bera, *Chem. Commun.*, 2008, 2511–2513; (*f*) H.-P. Lee, Y.-F. Hsu, T.-R. Chen, J.-D. Chen, K. H.-C. Chen and J.-C. Wang, *Inorg. Chem.*, 2009, **48**, 1263–1265; (*g*) H. Huang, A. L. Rheingold and R. P. Hughes, *Organometallics*, 2009, **28**, 1575–1578; (*h*) K. H. G. Mak, P. K. Chan, W. Y. Fan, R. Ganguly and W. K. Leong, *Organometallics*, 2013, **32**, 1053–1059; (*i*) A. L. Rheingold and R. P. Hughes, CSD Communication, 2020, CSD deposition number 2000767.

24 K. P. Huber and G. Herzberg, *Molecular Spectra and Molecular Structure, Vol. 4—Constants of Diatomic Molecules*, Van Nostrand Reinhold Company, New York, 1979.

25 J. Chandrasekhar and W. L. Jorgensen, *J. Chem. Phys.*, 1982, **77**, 5080–5089.

26 (*a*) D. J. Liston, C. A. Reed, C. W. Eigenbrot and W. R. Scheidt, *Inorg. Chem.*, 1987, **26**, 2739–2740; (*b*) Z. Xie, T. Jelínek, R. Bau and C. A. Reed, *J. Am. Chem. Soc.*, 1994, **116**, 1907–1913; (*c*) D. S. Bohle and Z. Chua, *Organometallics*, 2015, **34**, 1074–1084.

27 M. L. Neville, C. Chan, B. R. Barnett, R. E. Hernandez, C. E. Moore and J. S. Figueroa, *Polyhedron*, 2023, **243**, 116565.

28 A. W. Addison, T. N. Rao, J. Reedijk, J. van Rijn and G. C. Verschoor, *J. Chem. Soc., Dalton Trans.*, 1984, 1349–1356.